nature materials

SUPPLEMENTARY INFORMATION

https://doi.org/10.1038/s41563-019-0532-z

In the format provided by the authors and unedited.

Tunable quadruple-well ferroelectric van der Waals crystals

John A. Brehm[1,2,7], Sabine M. Neumayer[3,7], Lei Tao[1,4,7], Andrew O'Hara[1], Marius Chyasnavichus[3], Michael A. Susner[5], Michael A. McGuire[2], Sergei V. Kalinin[3], Stephen Jesse[3], Panchapakesan Ganesh[3], Sokrates T. Pantelides[1,2,6]*, Petro Maksymovych[3]* and Nina Balke[3]*

[1]Department of Physics and Astronomy, Vanderbilt University, Nashville, TN, USA. [2]Materials Science and Technology Division, Oak Ridge National Laboratory, Oak Ridge, TN, USA. [3]Center for Nanophase Materials Sciences, Oak Ridge National Laboratory, Oak Ridge, TN, USA. [4]University of Chinese Academy of Sciences & Institute of Physics, Chinese Academy of Sciences, Beijing, China. [5]Aerospace Systems Directorate, Air Force Research Laboratory, Wright-Patterson Air Force Base, OH, USA. [6]Department of Electrical Engineering and Computer Science, Vanderbilt University, Nashville, TN, USA. [7]These authors contributed equally: John A. Brehm, Sabine M. Neumayer, Lei Tao. *e-mail: pantelides@vanderbilt.edu; maksymovychp@ornl.gov; balken@ornl.gov

Tunable quadruple-well ferroelectric van-der-Waals crystals

John A. Brehm,[1,2‡] Sabine M. Neumayer,[3‡] Lei Tao,[1,4‡] Andrew O'Hara,[1] Marius Chyasnavichus,[3]

Michael A. Susner,[6] Michael A. McGuire,[2] Sergei V. Kalinin,[3] Stephen Jesse,[3] Panchapakesan Ganesh,[3]

Sokrates T. Pantelides,[1,2,5*] Petro Maksymovych,[3*] and Nina Balke[3*]

[1]Department of Physics and Astronomy, Vanderbilt University, Nashville, Tennessee 37235, USA

[2]Materials Science and Technology Division, Oak Ridge National Laboratory, Oak Ridge, Tennessee 37831, USA

[3]Center for Nanophase Materials Sciences, Oak Ridge National Laboratory, Oak Ridge, TN, USA

[4]University of Chinese Academy of Sciences & Institute of Physics, Chinese Academy of Sciences, Beijing 100190, China

[5]Department of Electrical Engineering and Computer Science, Vanderbilt University, Nashville, Tennessee, 37235, USA

[6]Aerospace Systems Directorate, Air Force Research Laboratory, Wright-Patterson Air Force Base, OH 45433 USA

[‡]Equally contributing authors

[*]Corresponding authors: pantelides@vanderbilt.edu (theory) and maksymovychp@ornl.gov,

balken@ornl.gov (experiment)

I. Structure and total energies in the vicinities of the two total-energy minima

The structure of the LP phase, which is characterized by the Cu atoms within the CIPS layers, is captured in Figure 1a. In the HP phase, the Cu atoms are displaced into the vdW gap and are bonded to S atoms in the adjacent layer (Figure 1b). In the HP case, then, the Cu atoms are tetrahedrally bonded to four S atoms with bond lengths equal to 2.47 Å for the S atom in the adjacent layer and 2.29 Å for the other three S atoms in the original layer. The tetrahedral Cu-S_4 coordination is seen in most chalcopyrites, for example Cu*B*S_2 (*B* = In, Ga, Fe, etc.), where the Cu-S bond length is 2.32 Å. No reconstruction or buckling of the sheets occur in the HP state.

The calculated total energies as functions of the *c*-lattice parameter at each of the two polar phases as shown in Figure S1a, with all other coordinates relaxed at each *c*-lattice parameter value, show two parabolic curves. These curves, like the results reported in the main text, were calculated using the ABINIT code, which employs norm-conserving pseudopotentials. The minimum of the HP phase is lower in energy by about 22 meV/f.u. The two curves were obtained with increased convergence requirements, relaxing to forces smaller than 5×10^{-10} eV/Å. Phonon calculations at the Γ point were undertaken from these tight relaxations, but yielded no negative frequencies, indicating that both structures are stable, which confirms that the energy barrier between the two minima is real, albeit quite small per formula unit. From the total-energy curves, the equilibrium c-lattice parameter is 13.09 Å for the Cu configuration in the layer and 12.87 Å for the configuration with Cu in the vdW gap, respectively.

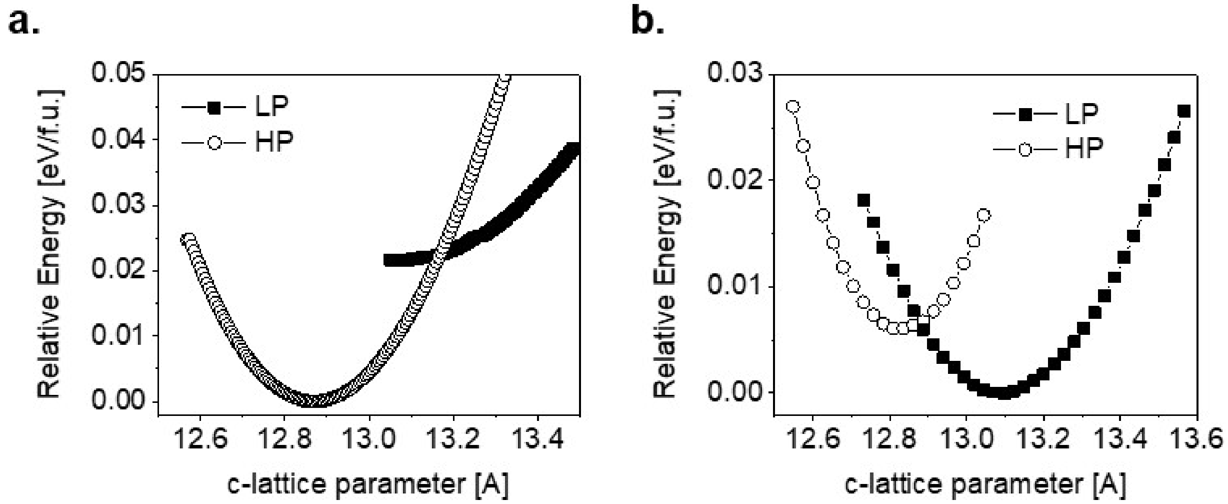

Figure S1. Total-energy curves for two structural phases with different Cu sites. Total energies as functions of the *c*-lattice parameter at each of the two Cu stable positions plotted relative to the minimum energy of the lower-energy state using (a.) ABINIT and (b.) VASP.

We note that, in You et al. (Sci. Adv. 5, eaav3780, 2019), the energy ordering of the HP and LP sites is reversed, though the differences are small: the total relative shift is ~30 meV. We verified that this difference is caused by the use of norm-conserving versus PAW pseudopotentials in the ABINIT and VASP computer codes, respectively. We calculated the two curves using the VASP code, keeping all other choices of functionals etc. the same as in the ABINIT code and obtained the results shown in Figure S1b. The equilibrium c-lattice parameters of the LP and HP phase are 13.09 Å and 12.86 Å, respectively. As noted in the main text, in the ABINIT calculations, the a, b, c, and β parameters of the LP phase have errors relative to the experimental values of 0.32%, 0.22%, -0.72%, and -0.01%, while using the PAW method in VASP the errors are -0.19%, -0.32%, -0.76%, and -0.19%, respectively, *i.e.,* the two sets of calculations have comparable accuracy in the structural parameters. The relative energy shift between the two calculations is small, ~25 meV. This result demonstrates that state-of-the-art DFT calculations cannot at this point tell us conclusively whether the HP or the LP is lower in energy. This difference, however, has no impact on any of the results reported in this paper as experiments cannot determine the true energy difference between the two states either.

II. Calculation of the quadruple-well curve by relaxing the c lattice parameter

In order to test the existence of the quadruple-well potential energy curve as function of Cu displacements when the lattice constants are allowed to relax at each point of the calculation, we performed additional calculations using the DFT-D3(BJ) method and the VASP simulation package. The existence of the quadruple-well potential-energy curve as function of Cu displacements is confirmed.

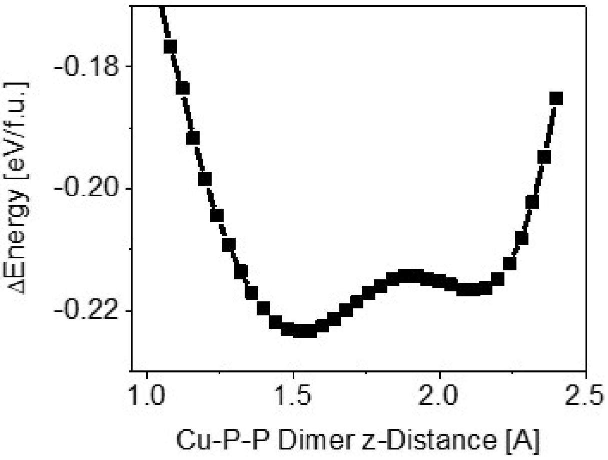

Figure S2. Relative energy calculations by continuously relaxing all lattice parameters. Relative energy as a function of Cu displacement relative to zero displacement. Each data point is the result of a total-energy calculation with relaxing lattice parameters including a, b, c, and β.

III. Correlation between ion-ion distances and polarization

The local energy minimum of the +LP state corresponds to an ion-ion distance of the Cu-P-P dimer of ~1.62 Å while the +HP state is at ~2.25 Å (Figure S3a). The corresponding z-polarization values can be extracted from Figure S1b. The change in the slope Figure S3b illustrates the marked effect that the location of the Cu atom has on the total (Berry plus ionic) *z*-polarization of CIPS, with the kink manifesting at the approximate Cu displacement coinciding with the first energy minima. After that point, the Cu atoms, under further displacement, come under the influence of the S atoms in the adjacent layer. It is this interaction that causes the polarization regime to change. Figure S3c and S3d show the polarization values of the local minima marking the low and high polarization phase as function of c-lattice parameter.

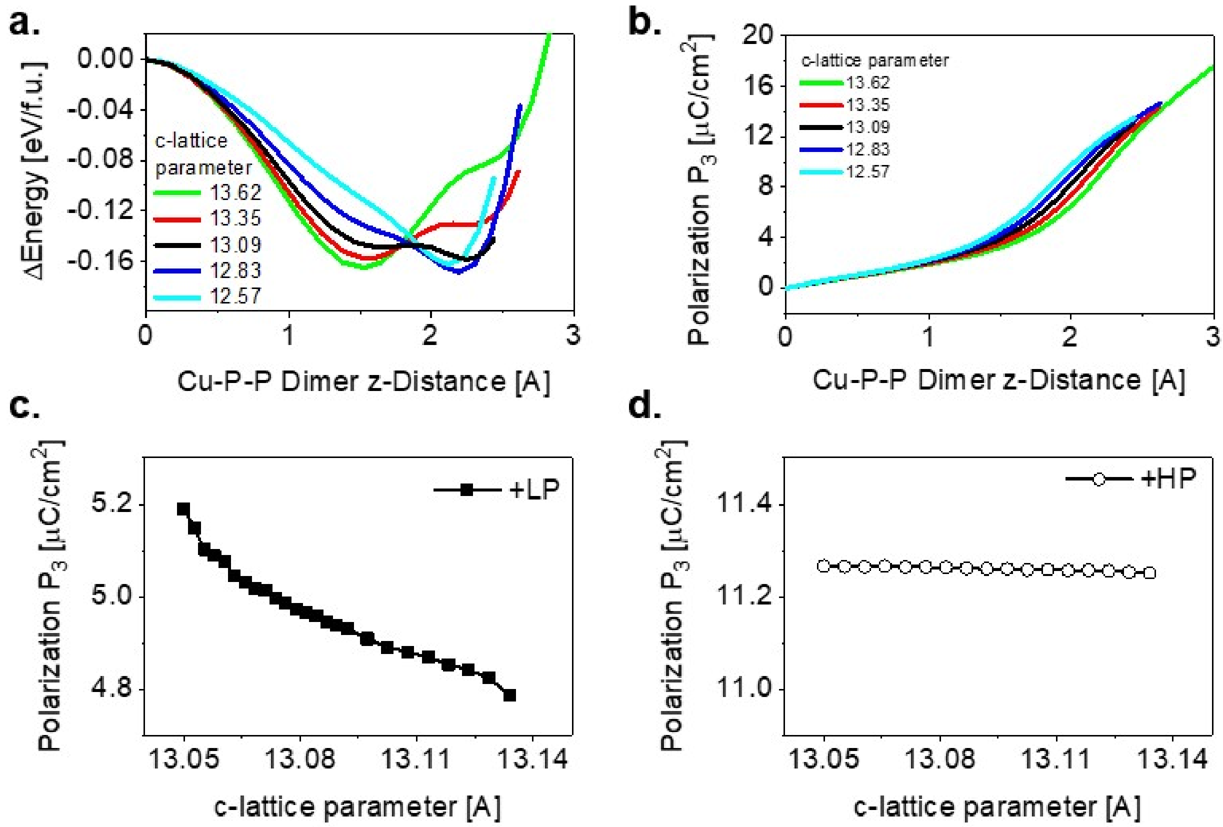

Figure S3. Quadruple-well as function of Cu displacement and resulting polarization as function of strain. For simulated c-lattice parameters of 12.57 Å, 12.83 Å, 13.09 Å, 13.35 Å, and 13.62 Å. (a.) the change in energy versus the displacement of Cu, and (b.) polarization versus the displacement of Cu. (c.) Polarization P_3 along the *z*-direction as a function of *c*-lattice parameter for the local-minima structures. For symmetry reasons, (c.) and (d.) only show the two positive polarization states aligned parallel to the *z*-direction. The relative range of the *y*-axis in (c.) and (d.) was kept constant for better comparison of polarization changes of +LP and +HP state.

IV. Separating CIPS and IPS response

The IPS phase is not ferroelectric and averages at an experimental value of zero serving as a reference point for the temperature and pressure-dependent results. Since more than half of the investigated area is the IPS phase, it overshadows the small piezoelectric constants measured in the CIPS phase. Therefore, a separation matrix was constructed based on the measured PFM response. The PFM phase (Figure S4a) was centered around zero between +/- π/2 by adding a phase offset (ϕ_{offset}). We calculated $-\cos(2\phi)$, where ϕ is the PFM phase, to give every ferroelectric domain in the CIPS phase a value of 1 (Figure S4b). The non-ferroelectric IPS phase appears as random noise. We performed a nearest-neighbor analysis around each pixel in a 3x3 cluster by calculating the average value of each sub-cluster moving through the image (Figure S4c). A CIPS pixel within a CIPS matrix would have the value 1. A pixel surrounded by half CIPS and half IPS would have a value of < 0.5. The threshold of value to select CIPS was chosen to be 0.8 (0.6 for T > 65 °C and 1.4 and 2.1 μN). The corresponding separation matrix (Figure S4d) and piezoelectric constant map (Figure S4e) are shown for the image taken at room temperature as an example.

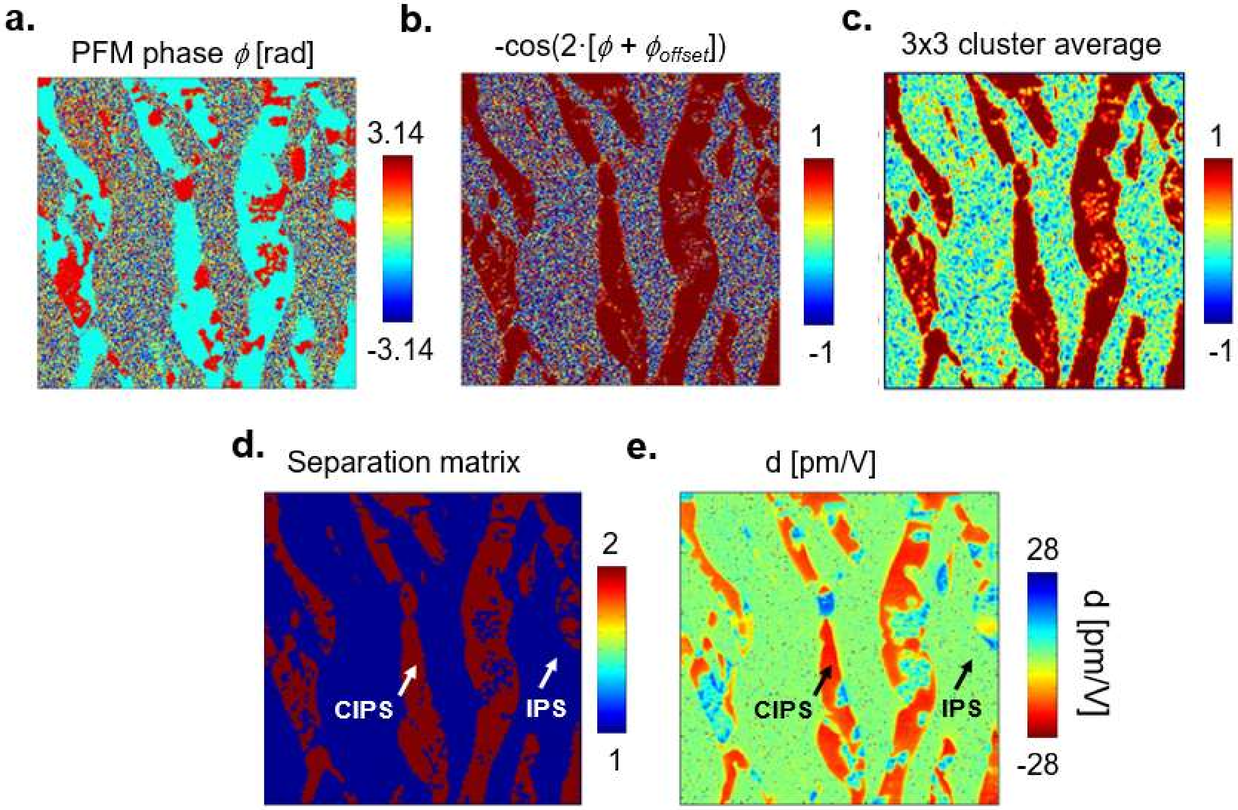

Figure S4. Construction of a separation matrix to distinguish CIPS and IPS phase. (a.) PFM phase measured at room temperature. (b.) Map for $-\cos(2\phi)$ after the PFM phase was centered around zero between +/- π/2 by adding an offset (ϕ_{offset}). (c.) Moving average of a 3x3 sub-cluster. (d.) Separation matrix based on a 0.8 threshold in image (c). (e.) Corresponding piezoelectric constant map

V. Temperature-dependent PFM measurements

Temperature-dependent PFM measurements in a 10x10 μm^2 area across the Curie temperature from which a smaller detail was extracted for the manuscript (Figure S5). The images were analyzed by separating CIPS from non-ferroelectric IPS phase and plotting the histograms for PFM on CIPS only.

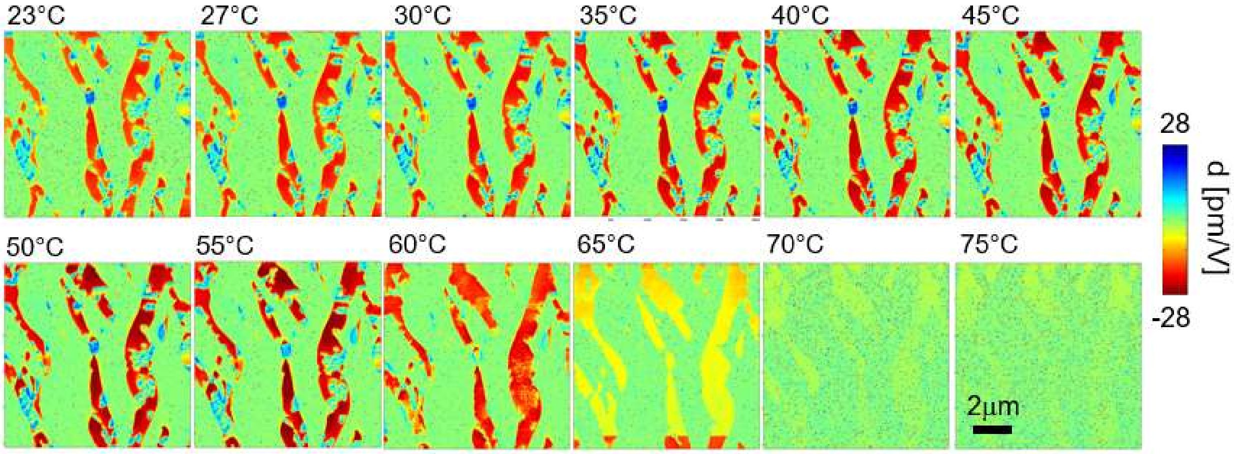

Figure S5. Temperature-dependent PFM measurements which are quantified to obtain values for the piezoelectric constant as function of temperature**.**

VI. Averaged IPS response as function of temperature and pressure

The non-ferroelectric IPS phase serves as reference point for the PFM measurements and change little as function of temperature (Figure S6a) and pressure (Figure S6b) suggesting no significant non-piezoelectric signal contributions. All distribution peaks are fitted using Gaussian functions whose widths determine the error bar for the measured average values extracted from the peak maximum positions.

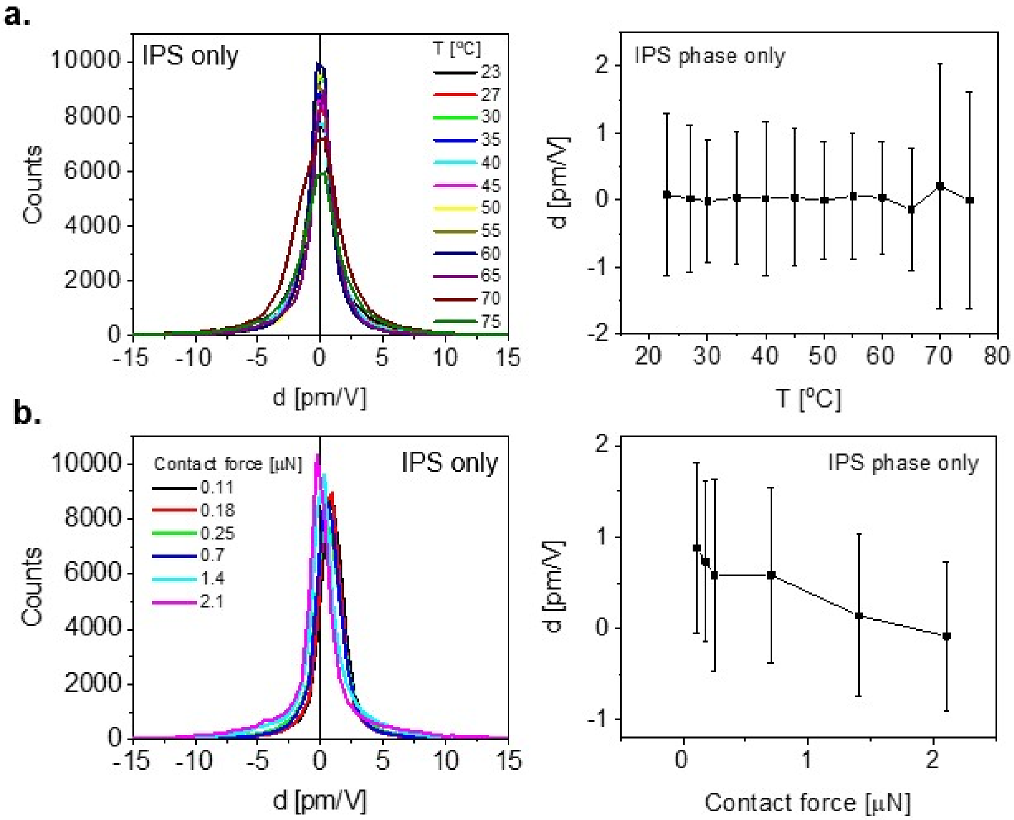

Figure S6. Temperature and pressure-dependent piezoelectric constant of the IPS phase. Histogram of the non-ferroelectric IPS response as function of (a.) temperature and (b.) pressure between cantilever and sample.

VII. Pressure-dependent PFM measurements

Pressure-dependent PFM measurements in a 10x10 µm^2 area from which a smaller detail was extracted for the manuscript (Figure S7). The images were analyzed by separating CIPS from non-ferroelectric IPS phase and plotting the histograms for PFM on CIPS only.

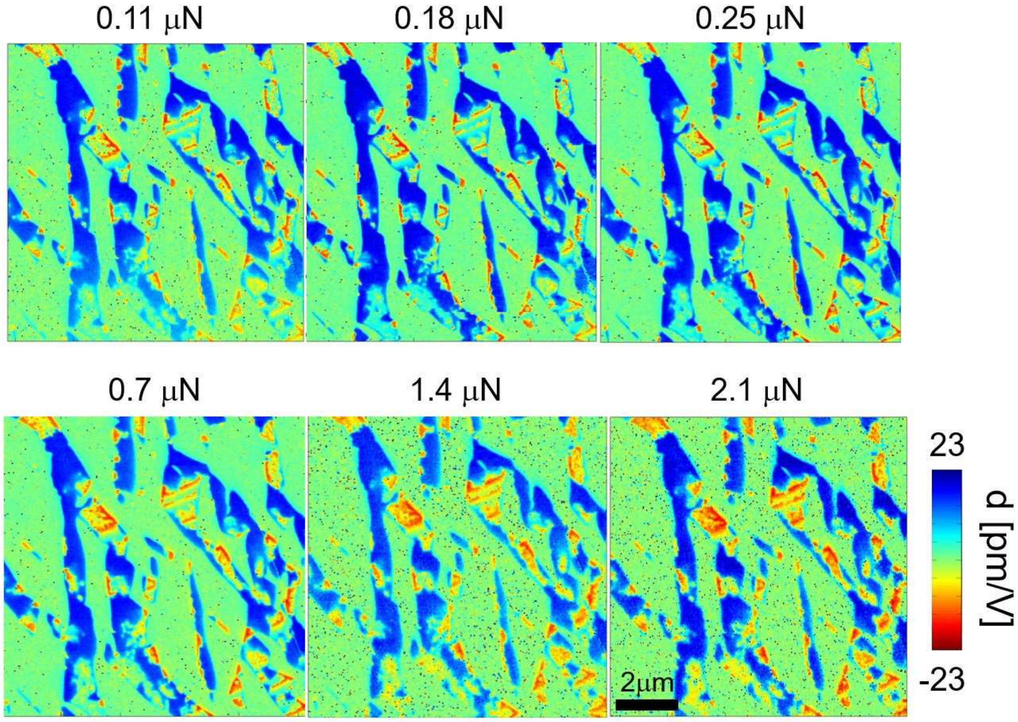

Figure S7. Pressure-dependent PFM measurements which are quantified to obtain values for the piezoelectric constant as function of contact force between PFM tip and sample.

VIII. Quantum molecular dynamics simulations

The processes of switching polarization states using an electric field are simulated using a supercell that contains four layers $CuInP_2S_6$ with a vacuum layer of 25 Å. An external electric field is applied along the *z* direction. To avoid the surface effect, we only show the positions of four Cu atoms in each of the two middle layers of a four-layer CIPS sample. At -173.15 °C (100 K), all the Cu atoms stay at the bottom of the layers and are jumping back and forth between HP and LP states because of thermal fluctuations (Figure S8a). Figure S8b and S8c show the switching processes at -73.15 °C (200 K) from the bottom to the top under an external electric field of 0.5 eV/Å and 1.0 eV/Å, respectively. At the end of 50 ps, three out of eight Cu atoms switch to the top under an electric field of 0.5 eV/Å while six out of eight Cu atoms switch under an electric field of 1.0 eV/Å. In Figure S8d we show the average Cu displacements in the *z* direction of eight Cu atoms in the two middle layers, according to Figure S8a-c.

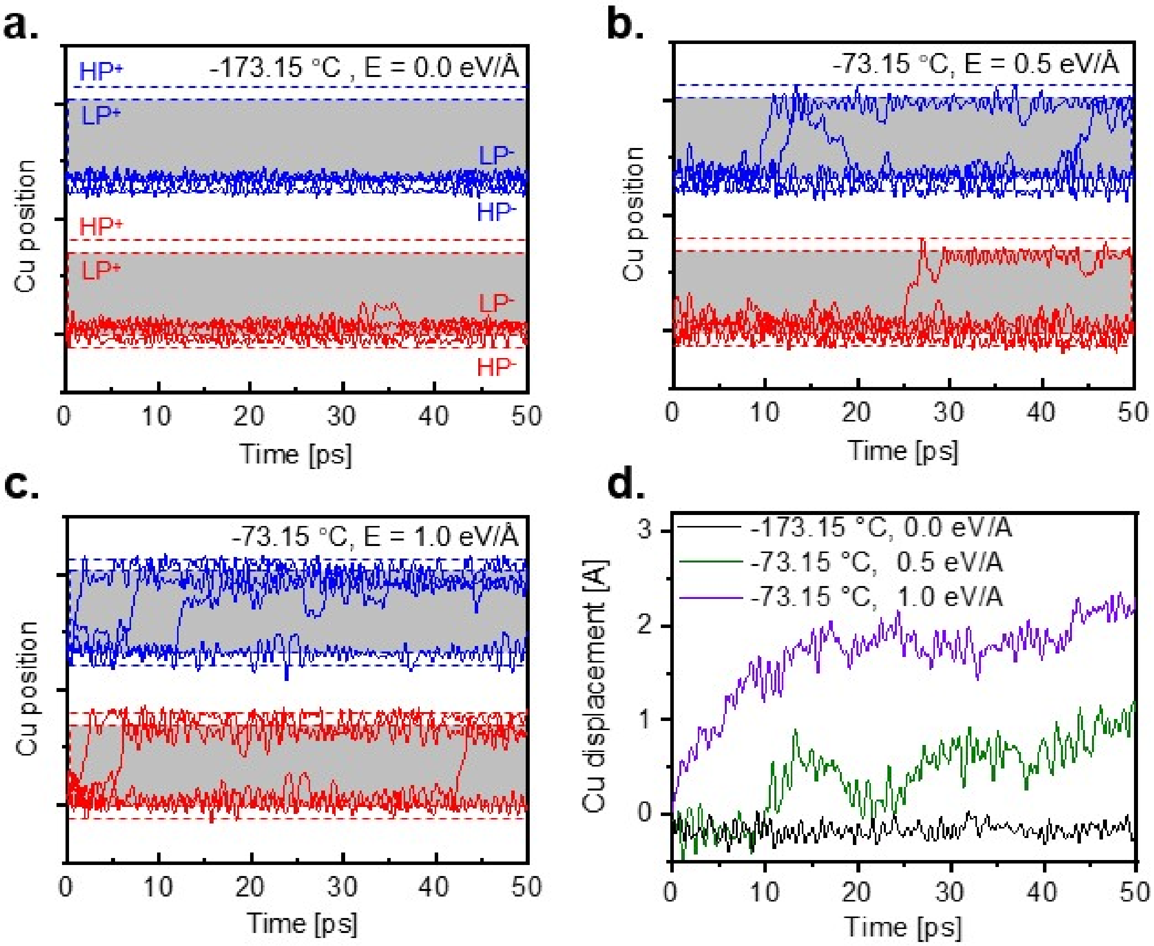

Figure S8. Dynamic simulations of bias-induced ferroelectric switching. Cu atom positions in each of the two middle layers of a four-layer CIPS sample. (a.) At -173.15 °C (100 K) without an electric field, the Cu atoms are jumping back and forth between HP and LP because of thermal fluctuations. Bias induced Cu position change at -73.15 °C (200 K) with an electric field of (b.) 0.5 eV/Å and (c.) 1.0 eV/Å. (d.) Average Cu displacements showing the response of Cu atoms to external electric fields along the *z* direction. The calculations were done using the VASP code.